Numerical Modeling of Meander and Eddy Formation in the Azores Current Frontal Zone

JÜRGEN KIELMANN AND ROLF H. KÄSE

Institut für Meereskunde an der Universität Kiel, D-2300 Kiel 1, West Germany

(Manuscript received 2 December 1985, in final form 8 October 1986)

ABSTRACT

Numerical experiments with an 11-level primitive equation, finite-difference model in a periodic channel are performed to analyze the properties of unstable finite-amplitude disturbances in an idealized Azores Current. Release of available potential energy due to baroclinic instability occurs preferentially on scales of about 100 km with a theoretical growth time of 8 days. At larger times, the combined effect of friction and nonlinear transfer between internal and external (depth integrated) mode and the distribution of energy among different wavenumbers of the initial disturbance determine the scale of the meandering jet. Cold water tongues with a meridional scale of several hundred km found in satellite images and hydrographic surveys east of the Azores are prescribed as initial disturbances. They develop into pairs of troughs and ridges dominated by cyclonic vortices on the poleward flank of the jet. Phase propagation is downstream at 2–4 km day^{-1}. Extremely strong frontogenetic enhancement of temperature occurs on the downstream side of the ridges, which gives rise to vertical velocities of order 10 m day^{-1}. Phase relations for baroclinically unstable waves indicate a mean poleward heat flux similar to observations in the Azores Current region.

1. Introduction

In large parts of the ocean, the mesoscale eddy-field dominates the circulation pattern. The question of how this variability is generated has been the subject of many studies, however, most of these studies concentrate on the aspects of meander and eddy formation connected with powerful western boundary currents (e.g., Robinson, 1983). It is now evident that oceanic regions which were considered to be part of the Sverdrup regimes also contain jetlike flows. These currents persist over long enough periods for baroclinic instability processes to develop (Niiler and Reynolds, 1984). Recent drifter experiments in the eastern North Atlantic (Krauss and Käse, 1984) reveal not only a concentration of eddy energy along the North Atlantic Current but also an enhanced activity in the vicinity of the Azores Current, which is regarded as a possible southeastward branch of the Gulfstream and the northern boundary of the inner subtropical gyre (Gould, 1985; Käse et al., 1985). The extensive meandering of the frontal zone is also evident in infrared satellite pictures. Figure 1a is a picture of the ocean surface temperature from approximately 31° to 39°N, 6° to 26°W taken from NOAA-7 on 10 March 1984. Two major temperature jumps are clearly visible: one is the temperature change from about 18° to 16°C water between 35° and 37°N and the other one is defined by the change from about 16°C to 14°C between 37° and 38.5°N. Figure 1b is a sketch of the principal form of the southern front, demonstrating the strong meandering in the zonal direction. The given scale suggests a meander wavelength of about 200 km.

The frontal zones and the associated zonal currents in this area are apparently a permanent feature. This is not only confirmed by hydrographic sections in different years (Käse et al., 1985, 86) but also inferred from climatological data using the β-spiral method (Olbers et al., 1985). Figure 2 is a picture of the estimated current field of the North Atlantic between 20° and 50°N in 100 m depth. The current field is very similar to Fig. 6a of Olbers et al. (1985) but is a less smoothed version. A broad eastward flowing current is quite evident between approximately 31° and 36°N which can be explained by the quasi-permanent existence of zonal fronts with varying position and meander development in this area. The thick black structures indicate the position of frontal zones as inferred from hydrographic surveys (from east to west: Käse et al., 1985; Gould, 1985; Mann, 1967).

To date, prognostic ocean circulation models have not simulated the occurrence of the Azores Current frontal zone and its high energy level. Linear wind-driven models (Müller and Frankignoul, 1981; Lippert and Käse, 1985) produce magnitudes of the energy which are too small by a factor of ten. Thus, baroclinic instability may be important for the mesoscale energy production in the Azores Current system.

Previous estimates of the role of baroclinic instability in the midlatitudes of the North Atlantic Ocean based on climatological hydrographic data (McDowell et al., 1983) predict that this process should not be important except in the region of the North Equatorial Current. However, synoptic maps of the density field (Käse et al., 1985) indicate that the geostrophic flow may be unstable to perturbations.

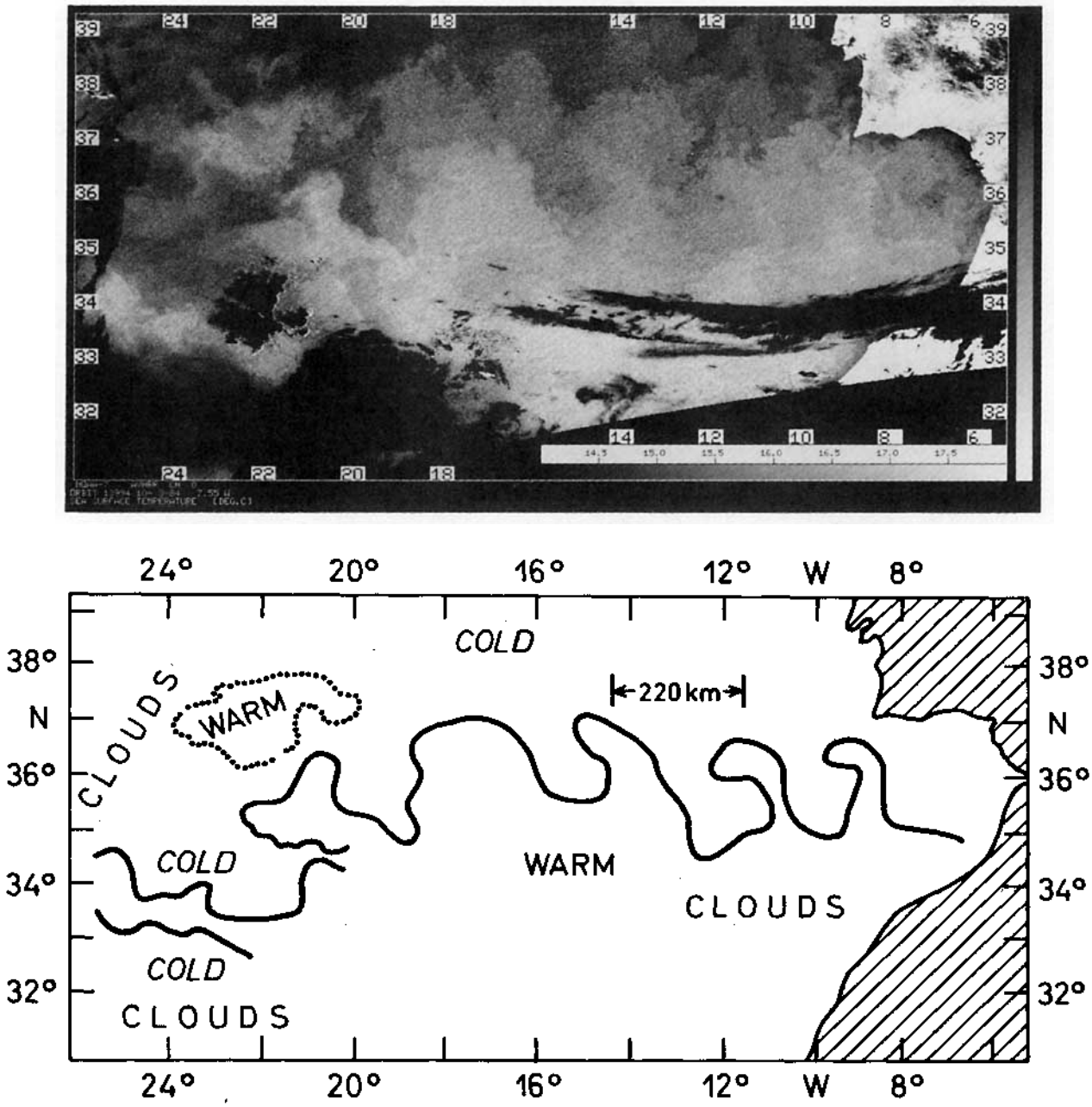

FIG. 1. (a) Surface temperatures computed from an infrared picture taken by satellite NOAA-7, at 1600 UTC 10 March 1984. (b) Sketch of the southern temperature front, 18° to 16°C, of the satellite picture (a) showing the intensive meandering features.

In this manuscript the development of finite-amplitude meanders on a jetlike flow from a given initial state is studied. The main purpose of this investigation is an analysis of the typical scales which develop from a localized disturbance of the flow, and which processes dominate the energy and the property distribution in the vicinity of the frontal zone.

2. The primitive equation model

In order to study the evolution of an idealized large scale meander as observed from the quasi-synoptic survey southeast of the Azores (Käse et al., 1985), the primitive equation model of Bryan (1969) as presented by Semtner (1974) is used. A primitive equation model is used in this investigation because strong ageostrophic effects are expected in the frontal zone due to confluence. Furthermore, future studies will include strongly varying topography such as the Gibbs Fracture Zone where the North Atlantic Current crosses the Mid-Atlantic Ridge as in Krauss (1986).

In contrast to the usual application of the Bryan (1969) model to large scale ocean circulation problems,

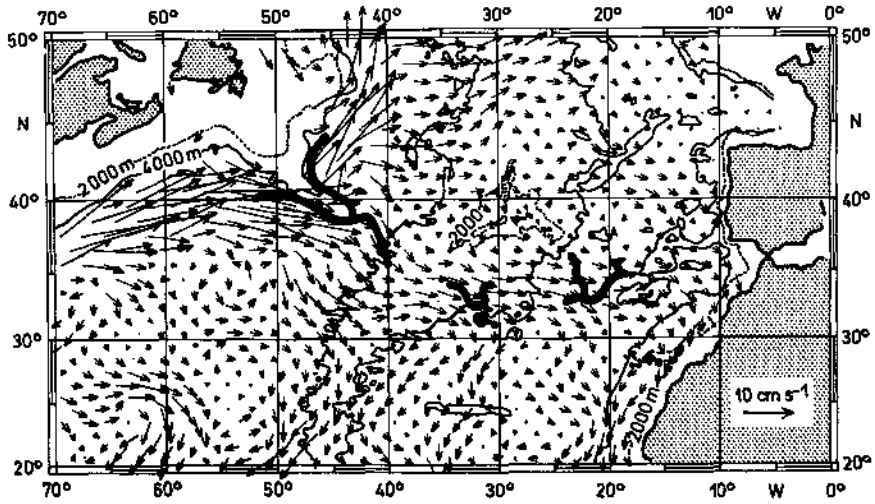

FIG. 2. Current pattern in 100 m depth of the North Atlantic as inferred from climatological hydrographic data by the β-spiral method (similar to Fig. 6a of Olbers et al., 1985). The dark structures show the position of frontal zones connected with features of the Gulf Stream extension as discussed by Gould, 1985.

the model is applied to the regional aspect of the Azores Current dynamics. The average first-mode internal Rossby radius in this area is 24–32 km (Emery et al., 1984). In order to achieve sufficient resolution for this area, the model domain is limited to an idealized version of the Azores Current region with closed north–south and periodic east–west boundaries. The effect of bottom topography is not considered in this study. The model is formulated in spherical coordinates with the center of the box at $\phi = 35°$N. For most of the numerical experiments, the domain extends 14.6° in the east–west direction (about 1332 km) and 5.9° in the north–south direction (about 655 km). The grid resolution is $\Delta\phi = 0.1°$ and $\Delta\lambda = 0.125°$, which corresponds to a grid size of about 10 km by 10 km, and results in roughly 7000 horizontal grid points. The vertical dimension is resolved in 11 levels, where the thickness of the first 5 layers is 100 m, the thickness of the second 5 layers is 300 m, and the last layer is 2000 m thick. A horizontally and vertically sheared jet in geostrophic balance is prescribed initially (see below) and the model is integrated in time.

To simplify the computations, salinity is kept constant, and an equation of state of the form

$$\rho/\rho_0 = 1 - \alpha T + \beta S_0 \tag{1}$$

is used with $\alpha = 10^{-4}\,(C°)^{-1}$, $\beta = 8 \times 10^{-4}$, $S_0 = 35.7$ and ρ_0 is some reference density ($\rho_0 = 1$).

The boundary conditions are

$$\left.\begin{aligned} \rho_0 A_M{}^v \frac{\partial}{\partial z}(u, v) = 0 \\ \rho_0 A_H{}^v \frac{\partial}{\partial z} T = 0 \end{aligned}\right\} \quad \text{at} \quad z = 0 \quad \text{and} \quad z = -H; \tag{2}$$

i.e., there is no momentum or heat flux through the bottom or surface.

At the northern (ϕ_a) and southern boundary (ϕ_b) a no-slip condition is imposed, and no flux of heat is allowed across either boundary.

$$\left.\begin{aligned} u, v = 0 \\ \partial T/\partial n = 0 \end{aligned}\right\} \quad \text{at} \quad \phi = \phi_a \quad \text{and} \quad \phi = \phi_b. \tag{3, 4}$$

At the western and eastern boundaries, periodic boundary conditions are applied for u, v, T. The vertical velocity, w, is computed diagnostically from the continuity equation.

In order to filter out external gravity waves, the rigid-lid approximation is used so that

$$w = 0 \quad \text{at} \quad z = 0. \tag{5}$$

At the flat bottom the vertical velocity vanishes,

$$w = 0 \quad \text{at} \quad z = -H. \tag{6}$$

The flow is separated into an external and an internal part. The external part is the vertically averaged flow for which a mass transport stream function ψ is defined.

By setting

$$\psi = \psi_a \quad \text{at} \quad \phi = \phi_a \quad \text{(southern boundary)} \tag{7}$$

$$\psi = 0 \quad \text{at} \quad \phi = \phi_b \quad \text{(northern boundary)}, \tag{8}$$

a net mass transport to the east ($\psi_a > 0$) or west ($\psi_a < 0$) is possible.

The initial conditions are chosen to represent an idealized version of an observed snap shot of the Azores Current (Fig. 3, after Käse et al., 1985). The general form of the idealized temperature distribution is

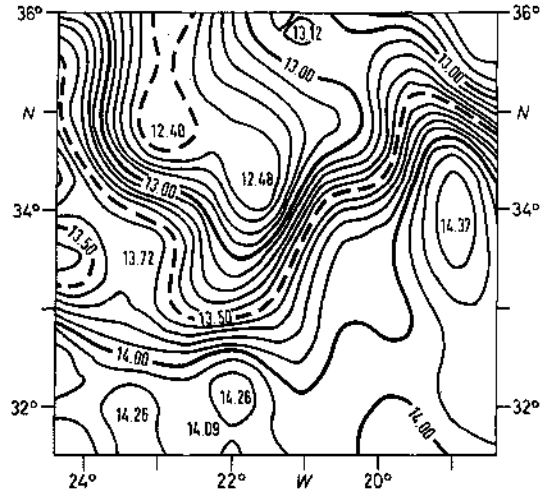

FIG. 3. Dynamic topography (dyn cm) of an Azores Current meander (25/1500 db, after Käse et al., 1985).

$$T = T_0 - \frac{\Delta T_s}{\cosh^2(z/D)}\left[\operatorname{erf}\left(\frac{y-\hat{y}}{L_y}\right) - 1\right] + \begin{cases} \Delta T_b \dfrac{z}{H_m}, & |z| \leq H_m \\ \Delta T_b, & |z| \geq H_m \end{cases} \tag{9}$$

where x is positive to the east, y to the north, z upward, and where $\hat{y}$ may be a function $\hat{y} = \hat{y}(x)$ allowing for an x-dependent departure from zonality. Without meandering $\hat{y} = \text{const} = B_y/2$, where B_y is the width of the model domain in y-direction. At the northern boundary T_0 is the surface temperature. The change from T_0 to $T_0 + \Delta T_s$ takes place in a narrow frontal zone of half-width L_y. There is a linear background temperature decrease from T_0 to $T_0 - \Delta T_b$ at a depth $z = -H_m$, which is kept constant down to the bottom at $z = -H$. Superimposed on this profile a deviation is described by the $\cosh^{-2}(z/D)$ function, with a depth scale D determining the vertical extension of the jet. The use of the error function allows for a change in the spacing of isotherms along a meridian.

The parameters related to the stratification in the Azores Current region are (Käse et al., 1985)

$$T_0 = 16°\text{C},\ \Delta T_s = 1°\text{C},\ \Delta T_b = 14°\text{C},\ H_m = 2000\ \text{m},$$
$$H = 4000\ \text{m},\quad D = 500\ \text{m},\quad L_y = 30\ \text{km}.$$

Thus, the temperature is 2°C below 2000 m. The surface water is 16° at the northern and 18° at the southern side of the frontal zone, and the 17° isotherm outcropping occurs at $y = \hat{y}$.

From the initial temperature distribution (9), the resulting geostrophic currents are

$$u = \frac{2g\Delta\rho D}{\sqrt{\pi} L_y f} e^{-[(y-\hat{y})/L_y]^2}\left[\tanh\left(\frac{z}{D}\right) + \tanh\left(\frac{H}{D}\right)\right] \tag{10}$$

$$v = u\frac{d\hat{y}}{dx} \tag{11}$$

where $\Delta\rho = 2\alpha T_s$. For $\hat{y} = \text{const}$, $v \equiv 0$ (zonal jet). For the parameters given, the maximum u-velocity is 22.1 cm s^{-1} along the jet axis. The depth integrated mean velocity is 1.7 cm s^{-1} and the total mass transport is 4.3 Sv (Sv $\equiv 10^6$ m^3 s^{-1}) across any (y, z)-section.

In order to prescribe a meander like perturbation similar to the observations, we specified $\hat{y}$ for two cases:

$$\hat{y} = \frac{1}{2}B_y + M_0\sqrt{2e}\left(\frac{x - x_M}{L_M}\right)e^{-[(x-x_M)/L_M]^2} \tag{12}$$

$$\hat{y} = \frac{1}{2}B_y + M_0 e^{-[(x-x_M)/L_M]^2}. \tag{13}$$

Equation (12) describes a local disturbance, which for positive M_0, produces a trough–ridge pair of amplitude M_0 with a length scale L_M (Fig. 4a). Equation (13) produces only a trough (or a ridge) of amplitude M_0 (Fig. 4b).

In order to study maximum growth rates as a function of wavenumber, a sinusoidal perturbation is superimposed on the purely zonal jet. The perturbation temperature added to (9) for this study is

$$T_{\sin}{}^n = A_0\frac{\Delta T_s}{\cosh^2(z/D)}\sin\left(\frac{2\pi}{B_x}nx\right)e^{-[(y-B_y/2)/L_y]^2} \tag{14}$$

where n is an integer wavenumber and B_x is the width of the periodic domain in x-direction. The geostrophic current perturbation on the zonal jet for $n = 6$ is shown in Fig. 4c. Figure 5 depicts the initial horizontal and vertical distribution of the temperature and current velocity of the unperturbed jet with the parameter values as stated above.

Figure 6a is a plot of the quasi-geostrophic potential vorticity gradient normalized by the planetary vorticity gradient. The potential vorticity gradient is negative in the upper 1000 m over most of the jet width and approaches unity outside the jet. Thus, the necessary condition for perturbations to grow in the sense of linear instability theory is satisfied.

Notice that the basic jet may be unstable in the upper 200 m also with respect to perturbations that draw upon the mean kinetic energy. This is obvious from Fig. 6b which is a plot of the normalized ambient vorticity gradient, of the gradient of the stretching term and of the total vorticity gradient including the planetary part. The horizontal curvature of the zonal flow enhances the beta effect in the center of the jet, and reduces the beta effect at the flanks which tends to destabilize the flow. The stretching term is always greater than the beta term at depths down to 1000 m for our choice of parameters. In this configuration, wave disturbances on the jet can only propagate eastward except in regions where the total vorticity gradient is positive.

Because the initial current field is not in complete

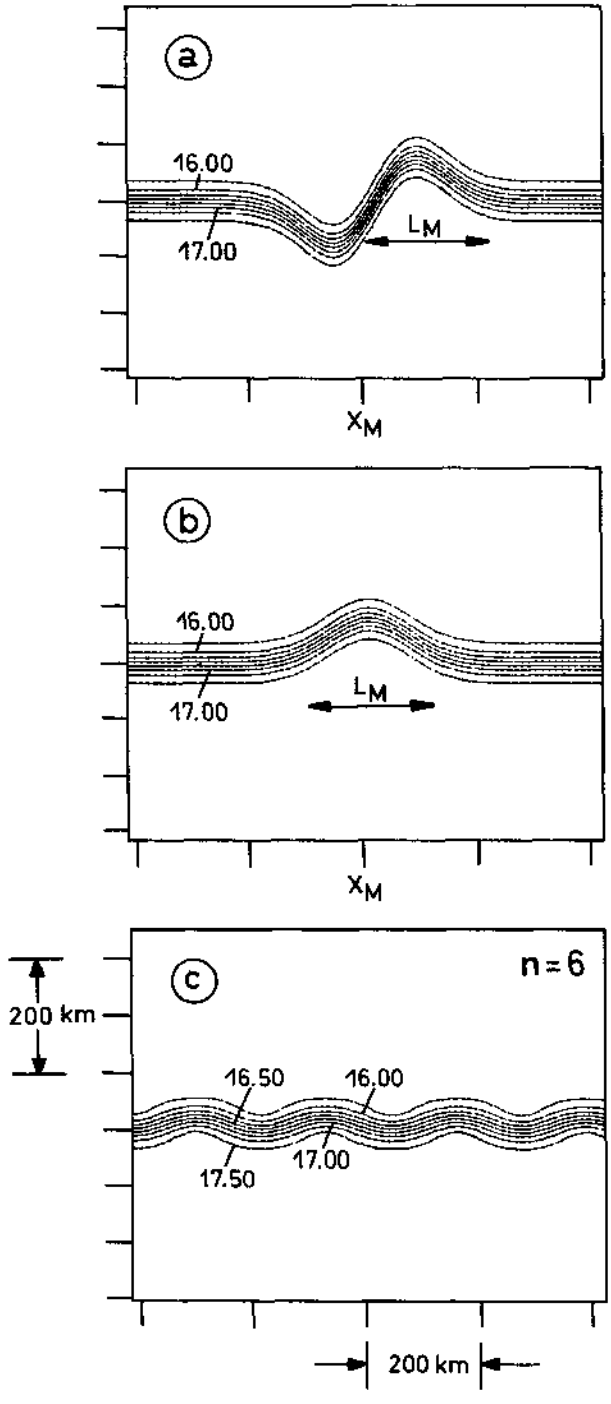

FIG. 4. Center portion of initial temperature disturbances on a geostrophic zonal jet at level 1 (50 m) for (a) double Gaussian (trough/ridge pair), (b) Gaussian (trough), and (c) sinusoidal (wavenumber 6).

geostrophic balance (although calculated geostrophically from the temperature field), the flow must adjust to nonlinear and frictional effects. The adjustment takes place in the first four days as can be seen from the time series of integrated kinetic energy (Fig. 7). Notice, the

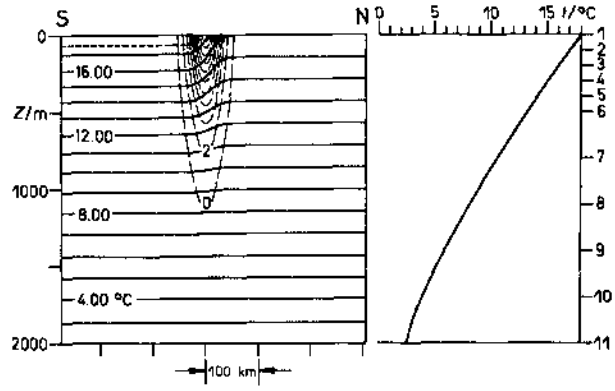

FIG. 5. Temperature and velocity section of the model jet (left) and vertical temperature profile with the position of the 11 levels indicated (right).

kinetic energy is oscillating with a period of about 21 hours during the first four days. The oscillations are due to inertial gravity waves which are damped in the model by use of a semi-implicit scheme for the Coriolis term. No such oscillations are evident after day 4.

The frictional parameters ($cm^2\ s^{-1}$) used in the model runs are

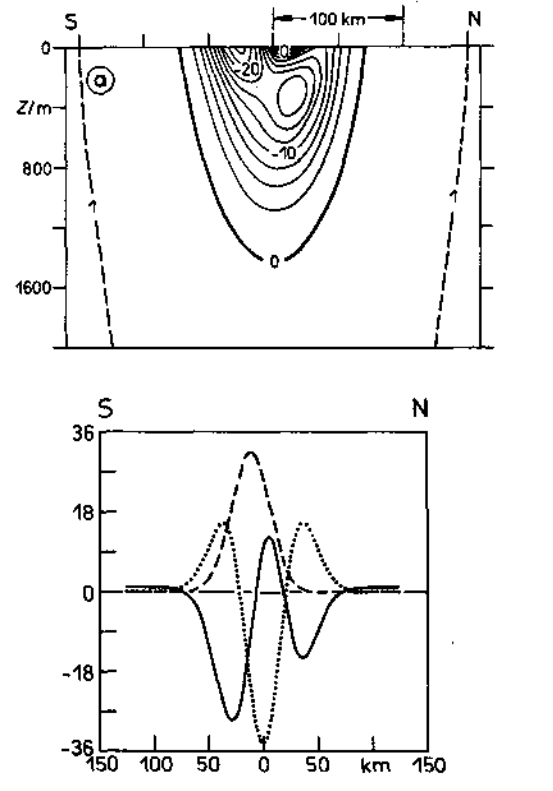

FIG. 6. (a) North/south section of the normalized potential vorticity gradient $q_y/\beta = 1 - (u_{yy} + (f_0^2 N^{-2} u_z)_z)/\beta$. (b) North/south distribution of u_{yy}/β (dotted line), stretching term $(f_0^2 N^{-2} u_z)_z/\beta$ (dashed line) and the total contribution q_y/β (full line) at the surface.

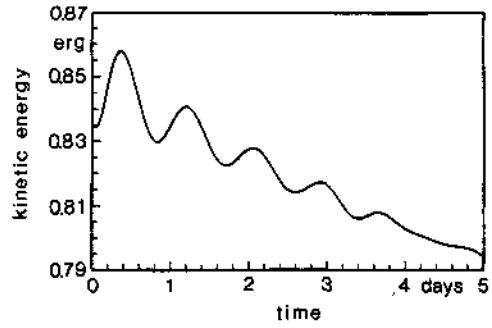

FIG. 7. Inertial adjustment of the model in the initial phase: box-integral of kinetic energy as function of time from Exp. 1, oscillation period is about 21 h (inertial period).

Horizontal diffusivity of momentum: $A_M{}^h = 10^6$

Vertical diffusivitiy of momentum: $A_M{}^v = 1$

Horizontal diffusivity of heat: $A_H{}^h = 10^4$

and

Vertical diffusivity of heat: $A_H{}^v = 1$.

The corresponding frictional layer for momentum at the southern or northern boundary is approximately 1 km thick. Because the grid resolution is 10 km, the boundary layer is not resolved. However, increasing $A_M{}^h$ by a factor of 10 damps all instabilities. After about two months of integration, a number of small scale disturbances became trapped along the northern and southern boundary which leads to unacceptable numerical errors. The integration time is certainly not long enough to reach a statistical equilibrium. However, neglection of external forcing (heating/cooling and wind stress) would result in an unrealistic dynamical balance, which could not maintain a permanent front. In most of the numerical experiments, two months of integration is sufficient to draw pertinent conclusions.

An additional problem in the computations occurs due to the numerical advection scheme (central differences), which causes "negative concentrations" of the advected quantities. The problem becomes especially serious if the advected quantity has strong gradients (e.g., Simons, 1980). The cell Reynolds number, $\mathrm{Re} = u\Delta x/A_M{}^h$, which should not exceed 2, may be as large as 20. For temperature advection, Re is even larger. As a consequence, numerical small scale noise can be seen in some of the numerical results, especially in the vicinity of the horizontal temperature fronts. Even higher order friction would not principally cure this problem. However, one remedy is to change the numerical advection scheme to upstream differencing with antiflux correction (Boris and Book, 1973; Smolarkiewicz, 1984). The method was not used here because it is too time consuming.

3. Initial growth of sinusoidal perturbations

The observations in the Azores current region suggest that the current is deflected southward during winter and early spring east of the island of Sao Miguel. The deflection is due to the penetration of cold watermasses from the north, which are driven by the large-scale windfields. Here, we do not attempt to simulate this but rather are interested in the development of the flow after the large scale deformation has come to a stop. The observed deviation from zonality connected with a dynamic low on the northern flank has a typical scale of 300 km (Fig. 4 after Käse et al., 1985).

It is seen from Fig. 1 that satellite observations in the Azores region suggest a typical meander scale of about 200–300 km downstream of a cold pool. In order to establish whether or not this scale is set by the scale of the fastest growing baroclinically unstable wave, the model is used to calculate the growth of sinusoidal linear perturbations on a zonal jet that has similar parameters of the Azores Current.

Figure 8 is a plot of three examples of model simulations with sinusoidal perturbations superimposed on the basic jet for wavenumbers $n = 3, 6, 12$ (444, 222, 111 km) with amplitude $A_0 = 0.29, 0.25, 0.16$, respectively. The A_0 (eq. 14) was made wavenumber-dependent in order to guarantee the same initial perturbation energy (10% of the basic jet kinetic energy). An increase in meander amplitude depends on the perturbation wavelength as expected both from linear theory and investigations by Holland and Haidvogel (1980) with a two layer quasi-geostrophic model. The stronger increase in meander amplitude at shorter wavelengths is clearly visible. There is also an eastward phase propagation in all three examples.

The box integrated total kinetic energy balance (Holland, 1975) in the initial phase (day 11) was calculated as a function of wavenumber n. The corresponding balance of the disturbance field was computed by subtracting the balance of the zonal jet run ($n = 0$). Changes in the energy level ($\dot{E}$) are due to an imbalance between release of potential energy by the work of pressure forces B and dissipation D:

$$\dot{E}(n) = B(n) + D(n), \quad n = 1, 2, \cdots. \tag{15}$$

This is plotted in Fig. 9a, where the individual terms have been normalized by the initial perturbation energy to give an inverse time scale (d^{-1}).

From $\dot{E}$ growth is found in the wavenumber range $n = 5$–22 (265–60 km wavelength) with a maximum at $n = 11$ (120 km). The fastest growth (8 days) is slower than the hypothetical growth (4 days) for the frictionless case ($\dot{E} = B$), where the potential energy released is totally transferred into the perturbation. Also, in the ideal case ($D = 0$), maximum growth is found at slightly higher wavenumbers ($n = 13$, 100 km).

The individual balance for the internal and external part is plotted in Fig. 9b and Fig. 9c. The principal

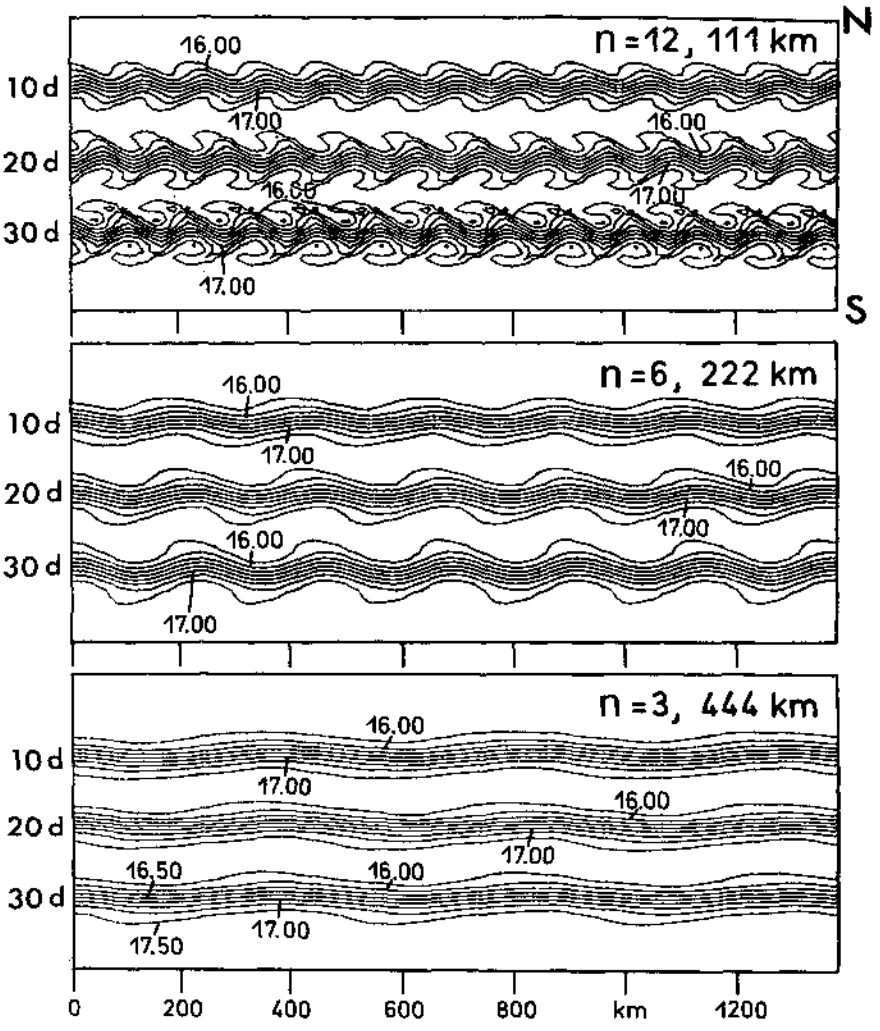

FIG. 8. Development of horizontal temperature distribution (°C) for sinusoidal initial perturbations at days 10, 20, 30 of wavenumbers n = 12, 6, 3.

source of energy for the internal mode is the buoyancy term $B_i = B$ while the external mode gains energy from the internal mode by nonlinear transfer N_i via horizontal and vertical advection. The internal mode looses energy in a broad range of wavenumbers $n < 14$ and $n > 20$ to the external mode. This indicates that the vertical structure of the initial disturbance tends to become more barotropic, while it tends to a more baroclinic nature in the range $14 < n < 20$. At the wavenumber of maximum growth the internal mode has the vertical structure of the basic jet and no nonlinear transfer to the external mode occurs.

If the energy growth rate $\dot{E}$ is converted to an amplitude growth rate by reducing the rate by a factor of two, the results may be compared to Holland and Haidvogel (1980). The shape of the growth rate curve is very similar to their examples. However, a remarkable difference lies in the position of the maximum which occurs at a wavelength of about 120 km. Although the primitive equation multi-level simulations are not immediately comparable to two layer quasi-geostrophic simulations, it is thought that the difference to the stronger shear in the top 500 m cannot be adequately accounted for by two layers.

A β–Rossby number $U/(\beta L^2)$ is of the same order (about 3) as in Holland and Haidvogel's standard case, whereas the square root of the Burger number R_d/L, based on the first mode, is slightly larger (about 0.76). However, since the first mode is not strongly dominant in our experiments, the shorter scale mirrors the shorter vertical scale of the baroclinic shear. It should be pointed out that the form of instability is not purely barotropic (due to horizontal shear) or baroclinic (due to vertical shear). This point will be addressed later when the model simulations for an idealized initial meander-disturbance are discussed.

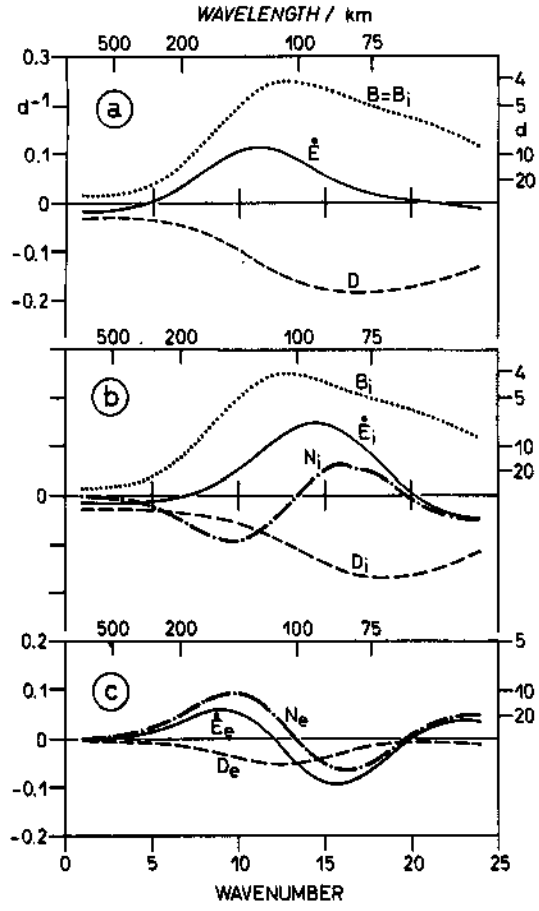

FIG. 9. Dominant terms of the perturbation energy balance as a function of wavenumber n (at day 11) normalized by the initial perturbation energy (to produce inverse time scales in d^{-1}). (a) Sum of internal (i) and external (e) mode according to Eq. (15). (b) Internal mode. (c) External mode where $B = B_i$ = release of potential energy by the internal mode; $\dot{E}$ = rate of change of kinetic energy; D = dissipation and N = rate of nonlinear transfer between internal and external mode ($N_i + N_e = 0$).

An initial jet with reversed current direction (to the west) gives different results. The maximum of $\dot{E}(n)$ at day 11 is found at wavenumber $n = 13$ and the growth rate is about twice as high, because the stabilizing effect of β is missing. The spectral energy balance is almost the same for wavenumbers $n < 7$, but the instability range extends to higher wavenumbers ($n = 26$).

The different results for eastward and westward basic jets are consistent with the linear instability theory and also with the thin jet theory of Flierl and Robinson (1984). The latter predicts that the growth rate spectrum has a critical scale

$$K_c^{-2} = \frac{\int\int u^2 dzdy}{\beta \int\int udzdy} \qquad (16)$$

based on the cross-jet properties. Waves with scale $k^{-1} < k_c^{-1}$ can grow due to instabilities. For the basic jet with the Azores Current parameters (eq. 10) Flierl and Robinson's (1984) theory predicts $2\pi k_c^{-1} = 410$ km (critical wavenumber $n_c = 3$). The long-wave approximation of Flierl and Robinson 1984 compares well with the results of Fig. 9a (dotted curve, $B = B_i$) for $n < 6$, but fails for $n > 6$. The short wave cutoff ($k = R_d^{-1}$) predicted by linear baroclinic instability theory (Pedlosky, 1979) is not clearly identified in the present calculations, probably due to frictional effects and to the difficulty of defining R_d for a surface-trapped jet.

4. Growth and propagation of isolated disturbances

a. Spectral composition of the initial stage

The initial development of disturbances depends critically on the dispersion of the medium and the distribution of initial energy in the spectral band of rapidly growing waves. As stated above, the growth rate can be computed from the positive part of the wavenumber spectrum of $\dot{E}$ by normalizing it with the initial perturbation energy. Since the major part of the discussion on the development of the disturbances refers to streamfunction or temperature patterns, it is more appropriate to divide the growth rate spectrum $G(n)$ of the kinetic energy by the square of the wavenumber n. The result $G\,n^{-2}$ is normalized to fit into [0, 1] and plotted in Fig. 10 (solid curve) together with the spectrum of the initial disturbance $S(n)$ (dashed curve) of Exp. 1, trough–ridge pair, (Table 1). At initial times, the theoretical response of a linear filter involving exponentially growing waves is the product $S(n)G(n)/n^2$ (dotted curve in Fig. 10). The maximum response is dominated by wavenumber $n = 6$ which corresponds to the observed wavelength of 220 km. About the same result is obtained for Exp. 2 (trough). Figures 11a and Figs. 11b are plots of the external streamfunction of Exp. 1 and 2 (Table 1) at day 0 and at day 50. The

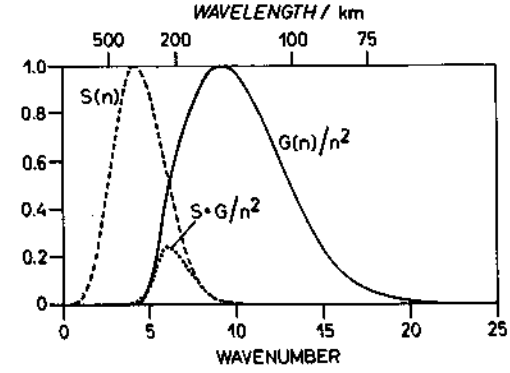

FIG. 10. Growth rate spectrum $G(n)n^{-2}$ (solid curve), computed from $\dot{E}$ of Fig. 9a and normalized (see text), initial normalized perturbation spectrum $S(n)$ of Exp. 1 (dashed curve) and product $S(n) \cdot G(n)n^{-2}$.

TABLE 1. Numerical experiments.

Exp.	M_0 (km)	L_M (km)	L_y (km)	Gaussian meander form: Single	Gaussian meander form: Double
1	75	100	30		*
2	−300	100	30	*	
3	−300	300	30	*	
4	−150	100	50		*

Sinusoidal perturbations of different wavelength on the zonal current with L_y = 30 km.

fastest growing wave (about 100 km wavelength) of Fig. 10 for these jet profiles has practically no measurable energy initially. It is expected that several scales will be present during meander development (Ikeda and Apel, 1981). The 200 km wavelength has the most prominent increase, with a propagation along the northward branch of the meander. The isolated disturbance has a strong phase coupling so that the shorter waves interfere constructively in the vicinity of the southward extremum, while the longer ones prevail in the outward branches. The spinup of the disturbances is due to the advection of relative vorticity. Thus, shorter waves emerge from the center of the jet and propagate downstream, while longer waves emerge from the less steep sides. Since the long-wave components grow more slowly, they are clearly visible only at later times. Another example is given by Fig. 11c with a still larger scale. This is typical of a situation where the shorter waves having small initial energy develop more rapidly due to the quasi-exponential growth (Exp. 3).

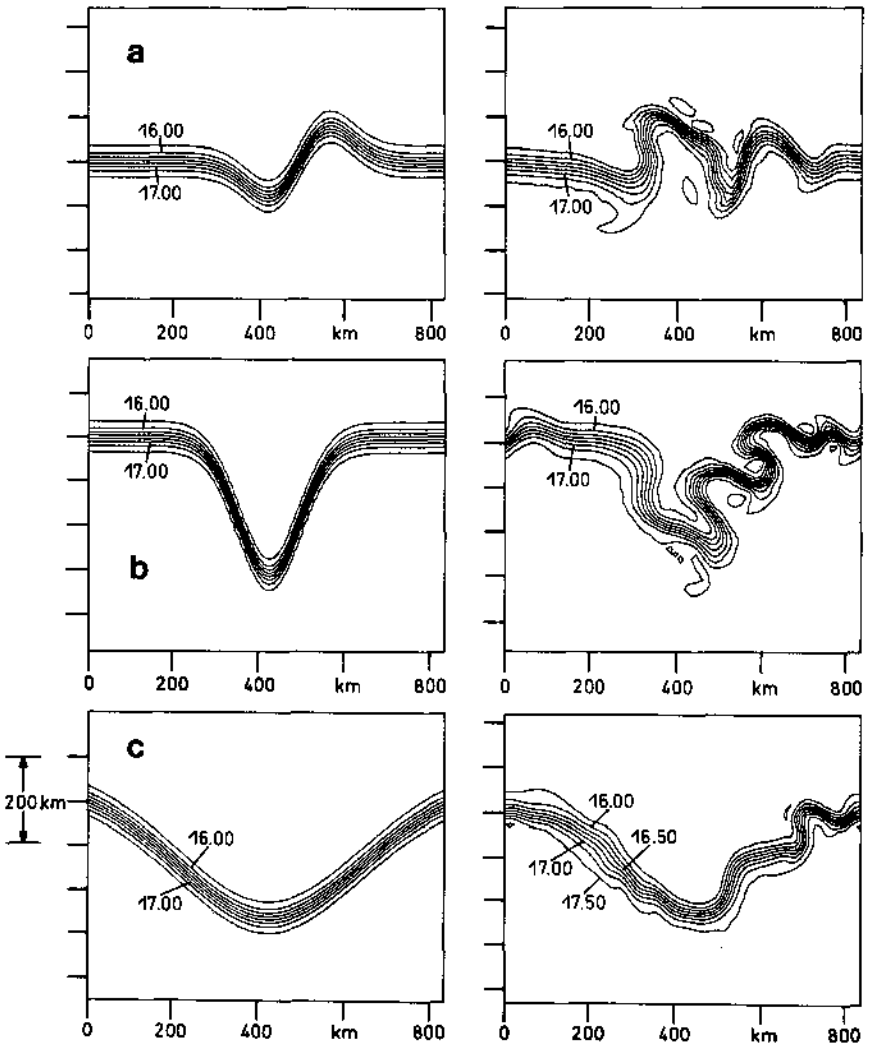

FIG. 11. Meander development from initial state (left panel) and at day 50 (right panel) for three different initial fields corresponding to (a) Exp. 1, (b) Exp. 2, (c) Exp. 3 with parameters given in Table 1.

b. Evolution of isolated disturbances

Remarkable meander formation in the northeast Atlantic is well known from infrared satellite data (see Fig. 1, also Hardtke, 1984). In this study the evolution of meanders and the detachment of an eddy is demonstrated by showing the temperature distribution of the top level of the model for Exp. 1 and Exp. 4 (50 m depth). Figure 12 is a plot of a sequence of isotherms $T(x, y)$ of Exp. 1, each ten days apart. The initial temperature field consists of a trough–ridge pair with M_0 = 75 km and a half-width of the jet (L_y = 30 km as in Fig. 4a) with cold water displacement to the south and warm water displacement to the north. This initially antisymmetric picture is changing rapidly as the warm water anomaly moves toward the northwest forming a wedgelike pattern by day 50. In the vicinity of the downstream flanks of the ridge, the temperature contrast has intensified to a sharp front. Figure 13 is a plot of isotherms of Exp. 4 with meander amplitude twice as high as in Exp. 1 (M_0 = −150 km, ridge–trough) and a half-width of the jet, L_y = 50 km. The snapshots are taken at 20 day intervals starting with day 20. A comparison between day 20 and day 60 at $x \approx 600$ km shows again a strong enhancement of the horizontal temperature gradient. A north–south section of the vertical velocity field at this point (not shown here) reveals downward vertical velocities of up to 10 m day^{-1} due to confluent currents. The intensive sharpening of the temperature gradient is similar to atmospheric phenomena where the formation of fronts associated with developing baroclinic disturbances is a common feature. For both experiments (Fig. 12 and Fig. 13) new trough–ridge pairs evolve simultaneously downstream with comparable warm front enhancement along the southward branch of the ridges. As expected, the dominant wavelength at day 70 is about 200 km for Exp. 1. Notice, that the leading waves at later times appear to have scales around 100 km. Also, at day 70, the first front starts to be modulated by a wave of about 100 km. This is also true for Exp. 4 (Fig. 13) where the 100 km scales are clearly visible at day 80. Also, by this time an eddy has detached from the jet at x = 500 km, trapping water masses of the frontal zone. Because the model has a limited horizontal resolution, the increasingly smaller scales connected with the frontogenesis mechanisms—apparently playing a crucial role in the further development of the system—can not be resolved.

The meanders are almost stationary in Fig. 12. By comparing the location of the ridge centers about a month apart it is possible to estimate the phase speed for the 200 km disturbance at about 2 cm s^{-1} to the east. The 100 km disturbance moves about 3.5 cm s^{-1}. Such phase lags could be measured in the velocity as well as the temperature records of a current meter array.

Figure 14a is a plot of the u,v-time series of Exp. 1 at two points A and B (defined in Fig. 12, day 10) 22 km apart. Figure 14b displays the corresponding temperature series. Points A and B are located east of the northward flowing branch of the initial meander, i.e., on the warm side. The temperature at A starts decreasing at about day 20, whereas at B it starts decreasing at day 33. The meridional velocity leads the temperature by roughly 90°. The phase speed estimated from the time series is 2 cm s^{-1}, corresponding to an apparent period of 116 days for the 200 km wavelength. This period compares favorably with the 138 day period of autocorrelation function analysis of the meridional component in Käse et al. (1985) and the NEADS cur-

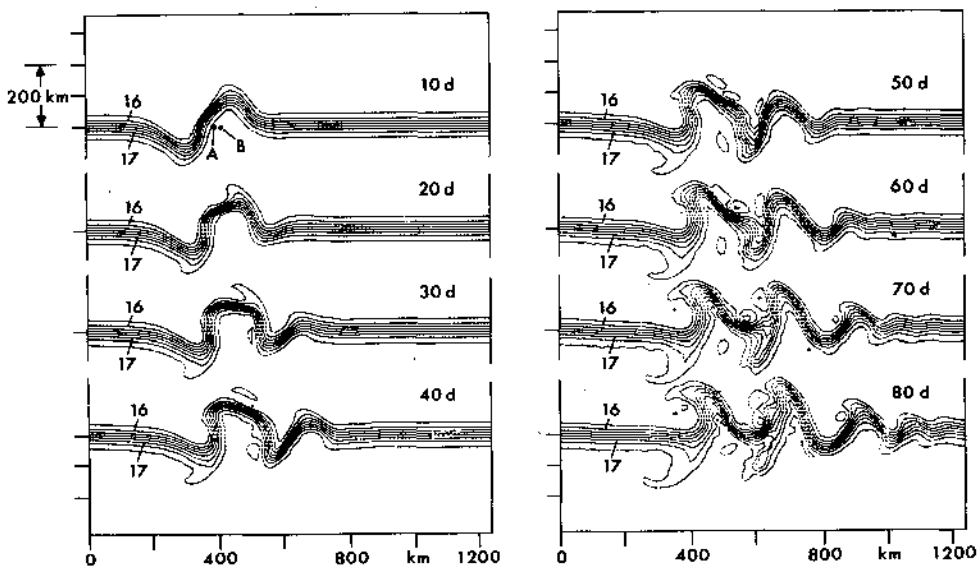

FIG. 12. Time evolution of temperature patterns at level 1 (50 m) for initial trough/ridge pair of Exp. 1. Locations A, B shown at day 10 are used for reference in Fig. 14. Meander amplitude: 75 km, horizontal scale: 100 km. Half-width of current: 30 km.

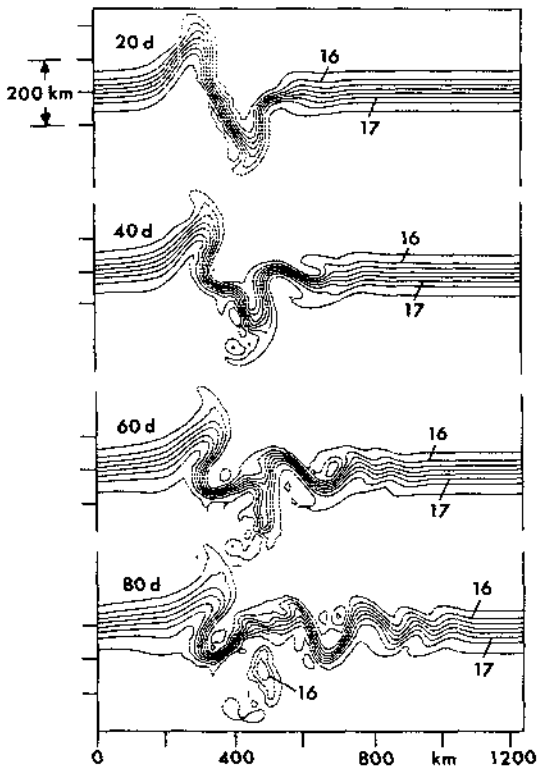

FIG. 13. Time evolution of temperature patterns at level 1 (50 m) for the initial ridge/trough pair of Exp. 4. Meander amplitudes: −150 km, horizontal scale: 100 km, half-width of jet: 50 km. The patterns are Hanning-smoothed to suppress small scale noise due to central differencing.

rent meter data (NEADS = North-East Atlantic Dynamics Studies, Müller and Zenk, 1983). However, phase propagation is not clear from the current measurements. Figure 15 displays the external (mass transport) streamfunction at day 70 for Exp. 1. A remarkable feature is the presence of 3 cyclonic vortices corresponding to cold water pools located poleward of the northward flank of the mean jet. This has also been observed in the numerical experiments of baroclinic instability in the atmosphere (Simmons and Hoskins, 1976). Each of these cyclones have a mass transport of about 50% of the jet transport. Contrary to that, the anticyclonic vortices are less strong.

The vertical structure of a north–south section of the zonal velocity component through the second cyclone is shown in Fig. 16. The isotachs reveal considerable phase shift with depth indicating the strong baroclinic nature of the process. The evolving temperature pattern is due to a phase lag between isotherms and streamlines, resulting from the secondary circulation of the growing waves. The phase relations for unstable baroclinic waves (Charney, 1947; Eady, 1949) are such that the poleward jet branch has an average warm advection and the equatorward branch an average cold advection, giving rise to a net poleward heat flux proportional to $\langle v'T' \rangle > 0$, which though small, is evident in these experiments. Figure 17 shows the zonally averaged, accumulated eddy correlations $B_y^{-1} \int_0^y \langle v'T' \rangle dy^*$ for day 70 at three depths (150, 250, 450 m). The total northward transport over the upper 500 m due to the three meander disturbances is 0.1 °C cm, a value which compares with 0.2 °C cm found by Käse et al. (1985) from eddy correlations in the Canary Basin.

Because of the mixed barotropic–baroclinic character of the instability process, Reynolds stress contributions $\langle u'v' \rangle$ should also be present. Figure 18 is a plot of the Reynolds stresses along a meridional section together with the zonally averaged flow at day 70 in the top level. The tilt of the trough–ridge systems gives rise to a negative correlation (Fig. 18). The total work done by the Reynolds stresses on the zonal mean flow tends to increase the mean kinetic energy. The process is similar to mixed instability processes in the atmosphere (Gill, 1982).

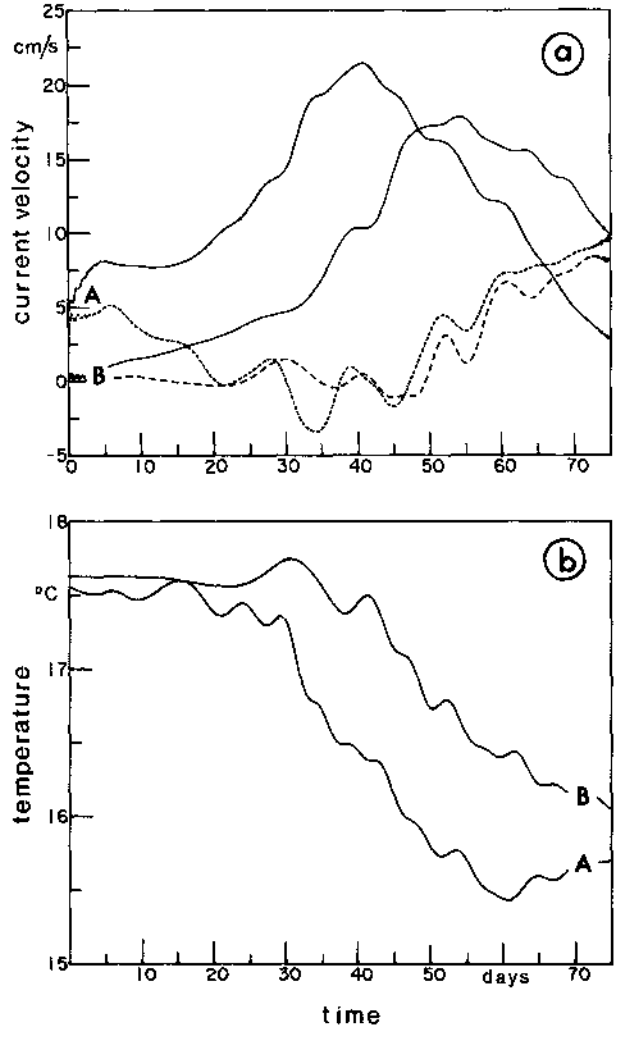

FIG. 14. Time series at two locations (A: x = 390 km, B: x = 412 km, Fig. 12) for (a) current velocity—east (full line) and north component (dashed line) and (b) temperature.

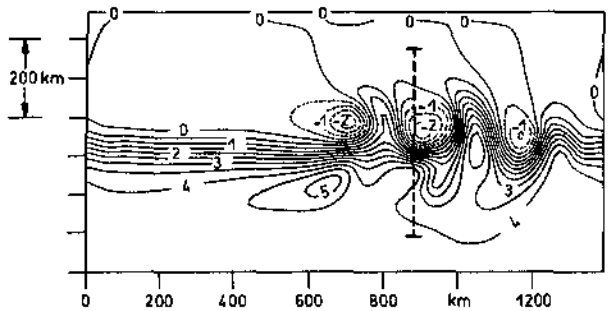

FIG. 15. Depth integrated streamfunction of Exp. 1 at day 70, showing the formation of closed cyclonic vortices at the northern flank of the zonal jet. The section at x = 900 km (dashed line) is referred to in Fig. 16.

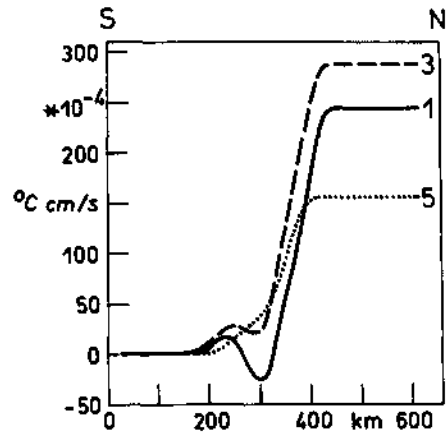

FIG. 17. Normalized cumulative meridional temperature transport $B_y^{-1}\int_0^y \langle v'T'\rangle dy^*$ at levels 1, 3, 5 (50, 250, 450 m).

5. Summary and conclusions

This investigation deals with properties of unstable disturbances of a thin jet with typical characteristics of the Azores Current. Numerical experiments were performed with an 11-level primitive equation finite difference model (Bryan, 1969; Semtner, 1974) in a periodic channel. Theoretical growth rates have been calculated for sinusoidal disturbances superimposed on a horizontally and vertically sheared jet which were allowed to develop to finite amplitude meanders. Growth was found for wavelengths in the range 50–300 km with a maximum growth rate at about 120 km and an amplitude e-folding of about 8 days. The computed scale of 120 km is considerably smaller than would be suggested by a two-layer quasi-geostrophic model as used by Holland and Haidvogel (1980). According to instability theory (Gill, 1982), an equivalent first-mode Rossby radius of 33 km, results in a dominant wavelength of order 200 km. However, the initial jet is trapped in the upper 1000 m. A modal decomposition involves at least 3 baroclinic modes leading to an effective deformation radius of 15–20 km. Thus, the expected dominant scale is about 100 km which is the scale found in the numerical simulations that have the fastest growth.

The combined effect of friction and nonlinear transfer between the internal and external modes together with the initial distribution of energy among different wavenumbers determine the scale of the meandering jet at larger times. A prominent feature in all simulations was a growing vertical penetration scale resulting from nonlinear redistribution of internal kinetic energy into the external mode. The increasingly more barotropic nature of eddies is also found in two-layer experiments, as noted by Rhines (1977).

Several experiments involving meander formation from isolated initial disturbances have been performed. Initial perturbations having characteristic scales of cold water tongues east of the Azores develop into pairs of

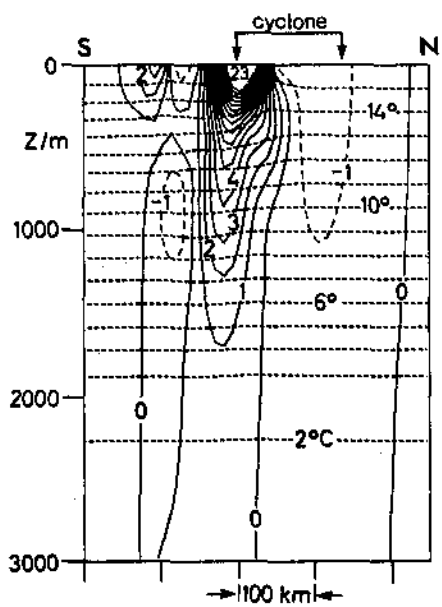

FIG. 16. Meridional section defined in Fig. 15 of the east component of velocity and temperature at day 70 (Exp. 1), showing increased depth scale of the perturbed jet.

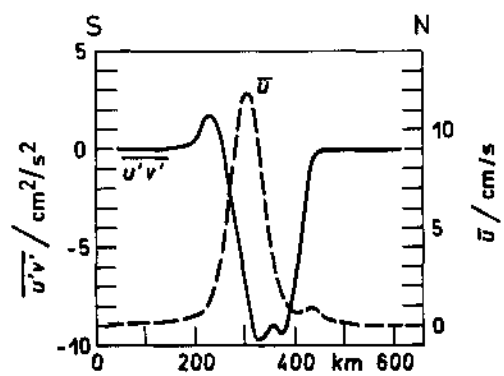

FIG. 18. Meridional profile of zonally averaged momentum flux $\langle u'v'\rangle$ (full line, scale on left hand side) and zonal mean velocity $\langle u\rangle$ (dashed line, scale on right hand side).

troughs and ridges. The circulation is dominated by cyclonic vortices on the poleward flank of the eastward flowing jet, whereas anticyclonic activity is suppressed. Depending on the spectral composition of the initial deformation, the scale of the meander is between 100 and 200 km, since the growth rate spectrum is not sharply peaked. Phase velocities are generally directed eastward and are small. The 200 km meander moved at a mean speed of about 2 cm s^{-1}, corresponding to a period of roughly 120 days. The smaller meanders travel ahead of larger scale disturbances with a phase speed of 3.5 cm s^{-1} for the 100 km scale. Typical phase relations for baroclinically unstable disturbances resulted in a poleward heat flux and Reynolds stress contributions which have been shown to influence the structure of the mean properties of the jet.

A striking feature was the extremely strong frontogenetic enhancement of temperature contrasts in the vicinity of the downstream flanks of the ridges. The associated secondary circulation reveals strong vertical velocities of the order 10 m day^{-1}. Vertical circulation cells of this strength can not be dealt with in quasi-geostrophic models and require an improved numerical advection scheme for the primitive model used in our experiments. The experiments described here revealed a more realistic picture of a meandering jet as can be explained by low (vertical) resolution quasi-geostrophic models. Nevertheless, this study is restricted to some idealized cases with parameters of the Azores Current region. After having improved the properties of the numerical model, especially by applying upstream differencing with antiflux correction to the advection terms, it may be worthwhile to use the model with the observed initial conditions of mesoscale experiments. In view of the increasing amount of information supplied by satellite techniques it should be possible to judge the importance of the instability processes in frontal regimes by monitoring the evolution of meanders and eddies and use the improved numerical model to better understand the underlying dynamics.

Acknowledgments. The assistance of S. Trier and A. Schurbohm in the preparation of the manuscript as well as the courtesy of M. Wenzel to supply us with the current pattern used in Fig. 2 is gratefully acknowledged. Thanks go also to an anonymous reviewer who pointed out an inconsistency in the growth rate calculations. This work was supported by the Deutsche Forschungsgemeinschaft, Bonn-Bad Godesberg (SFB 133).

REFERENCES

Boris, J. P., and D. L. Book, 1973: Flux corrected transport I: SHASTA, a fluid transport algorithm that works. *J. Comput. Phys.*, **11**, 38–69.

Bryan, K., 1969: A numerical method for the study of the circulation of the world ocean. *J. Comput. Phys.*, **4**, 347–376.

Charney, J. G., 1947: The dynamics of long waves in a baroclinic westerly current. *J. Meteor.*, **4**, 135–163.

Eady, E. T., 1949: Long waves and cyclone waves. *Tellus*, **1**, 33–52.

Emery, W. J., W. G. Lee and L. Magaard, 1984: Geographic and seasonal distribution of Brunt–Väisälä frequency and Rossby radii in the North Pacific and North Atlantic. *J. Phys. Oceanogr.*, **14**, 294–317.

Flierl, G. R., and A. R. Robinson, 1984: On the time dependent meandering of a thin jet. *J. Phys. Oceanogr.*, **14**, 412–423.

Gill, A. E., 1982: *Atmosphere–Ocean Dynamics. Int. Geophys. Ser.*, Vol. 30, Academic Press, 662 pp.

Gould, W. J., 1985: Physical oceanography of the Azores front. *Progress in Oceanography*, Vol. 14, Pergamon, 167–190.

Hardtke, P. G., 1984: Zur Abbildung ozeanischer Bewegungsvorgänge in Satelliteninfrarot-und Radaraltimeterdaten. *Z. Flugwiss. Weltraumforsch.* 8, Heft 5.

Holland, W. R., 1975: Energetics of baroclinic oceans. *Numerical Models of Ocean Circulation*, 168–177. National Academy of Sciences, Washington DC.

——, and D. B. Haidvogel, 1980: A parameter study of the mixed instability of idealized ocean currents. *Dyn. Atmos. Oceans*, **4**, 185–216.

Ikeda, M., and J. R. Apel, 1981: Mesoscale eddies detached from spatially growing meanders in an eastward-flowing oceanic jet using a two-layer quasi-geostrophic model. *J. Phys. Oceanogr.*, **11**, 1638–1661.

Käse, R. H., W. Zenk, T. B. Sanford and W. Hiller, 1985: Currents, fronts and eddy fluxes in the Canary Basin. *Progress in Oceanography*, Vol. 14, 231–257.

——, J. F. Price, P. L. Richardson and W. Zenk, 1986: A quasi-synoptic survey of the thermocline circulation and water mass distribution within the Canary Basin. *J. Geophys. Res.*, **91**(C8), 9739–9748.

Krauss, W., 1986: The North Atlantic Current. *J. Geophys. Res.*, **91**(C4), 5061–5074.

——, and R. H. Käse, 1984: Mean circulation and eddy kinetic energy in the eastern North Atlantic. *J. Geophys. Res.*, **89**(C3), 3407–3415.

Lippert, A., and R. H. Käse, 1985: Stochastic wind forcing of baroclinic Rossby waves in the presence of a meridional boundary. *J. Phys. Oceanogr.*, **15**, 184–194.

Mann, C. R., 1967: The termination of the Gulf Stream and the beginning of the North Atlantic Current. *Deep-Sea Res.*, **14**, 337–359.

McDowell, S., P. B. Rhines and T. Keffer, 1983: North Atlantic potential vorticity and its relation to the general circulation. *J. Phys. Oceanogr.*, **12**, 1417–1436.

Müller, P., and C. Frankignoul, 1981: Direct atmospheric forcing of geostrophic eddies. *J. Phys. Oceanogr.*, **11**, 287–308.

Müller, T. J., and W. Zenk, 1983: Some Eularian current measurements and XBT–sections from the North East Atlantic October 1980–March 1982. Ber. Inst. Meereskd. Univesity of Kiel, No. 114.

Niiler, P. P., and R. W. Reynolds, 1984: The three-dimensional circulation near the Eastern North Pacific subtropical front. *J. Phys. Oceanogr.*, **14**, 217–230.

Olbers, D. J., M. Wenzel and J. Willebrand, 1985: The inference of North Atlantic circulation patterns from climatological hydrographic data. *Reviews of Geophysics*, **23**, 313–356.

Pedlosky, J., 1979: *Geophysical Fluid Dynamics.* Springer–Verlag, 624 pp.

Rhines, P. B., 1977: The dynamics of unsteady currents. *The Sea*, Goldberg et al., Eds., Vol. 6, Chap. 7, Wiley-Interscience.

Robinson, A. R., 1983: *Eddies in Marine Science.* Springer–Verlag, 620 pp.

Semtner, A. J., 1974: An oceanic general circulation model with bottom topography. Technical Report No. 9., Dept. of Meteorology, University of California.

Simmons, A. J., and B. J. Hoskins, 1976: Baroclinic instability on the sphere: Normal modes of the primitive and quasi-geostrophic equations. *J. Atmos. Sci.*, **33**, 1454–1477.

Simons, T. J., 1980: Circulation models of lakes and inland seas. *Can. Bull. Fisheries and Aquatic Sci.*, No. 203, 145 p.

Smolarkiewicz, P. K., 1984: A fully multidimensional positive definite advection transport algorithm with small implicit diffusion. *J. Comput. Phys.*, **54**, 325–362.